PAPER

WILEY Terra Nova

Provenance record of late Maastrichtian–late Palaeocene Andean Mountain building in the Amazonian retroarc foreland basin (Madre de Dios basin, Peru)

Mélanie Louterbach[1] (iD) | Martin Roddaz[2] | Pierre-Olivier Antoine[3] | Laurent Marivaux[3] | Sylvain Adnet[3] | Julien Bailleul[4] | Elton Dantas[5] | Roberto Ventura Santos[5] | Farid Chemale Jr[5] | Patrice Baby[2] | Caroline Sanchez[2] | Ysabel Calderon[2,6]

[1]REPSOL Exploración S.A., Madrid, Spain

[2]Géosciences-Environnement Toulouse, Université de Toulouse, UPS (SVT-OMP); CNRS/IRD, Toulouse, France

[3]Institut des Sciences de l'Évolution de Montpellier (ISE-M, UMR 5554, CNRS/UM/IRD/EPHE), Université de Montpellier, Montpellier, France

[4]Basins-Reservoirs-Resources, Département Géosciences, UniLaSalle, Beauvais, France

[5]Laboratório de Geocronologia, Instituto de Geociências, Universidade de Brasília, Brasília, DF, Brazil

[6]PERUPETRO S.A., Lima, Peru

Correspondence
Dr. Mélanie Louterbach, Respol Exploración, Madrid, Spain.
Emails: melanie.louterbach@repsol.com; melanie.louterbach@hotmail.fr

Abstract

Biostratigraphic, sedimentological and provenance analyses suggest that a proto-Andean Cordillera already existed in southern Peru by late Maastrichtian–late Palaeocene times. A 270-m-thick stratigraphic section shows changes in depositional environments from shallow marine (early Maastrichtian) to non-marine (late Maastrichtian) then back to estuarine (late Palaeocene) conditions. An erosional surface separates lower Maastrichtian from upper Maastrichtian deposits. Above this surface, the late Maastrichtian unit exhibits moderately developed palaeosols and synsedimentary normal faults. The sedimentary evolution is accompanied by a decrease in sedimentation rate and by changes in provenance. Shallow marine lower Maastrichtian deposits have a cratonic provenance as shown by their low $\varepsilon Nd(0)$ values (−15 to −16) and the presence of Precambrian inherited zircon grains. The upper Maastrichtian deposits have a mixed Andean and cratonic origin with $\varepsilon Nd(0)$ values of ~12.6 and yield the first Cretaceous and Permo-Triassic zircon grains. Estuarine to shallow marine upper Palaeocene deposits have an Andean dominant source as attested by higher $\varepsilon Nd(0)$ values (−6 to −10) and by the presence of Palaeozoic and Late Cretaceous zircon grains. The changes in depositional environments and sedimentation rates, as well as the shift in detrital provenance, are consistent with a late Maastrichtian–late Palaeocene period of Andean mountain building. In agreement with recently published studies, our data suggest that an Andean retroarc foreland basin was active by late Maastrichtian–late Palaeocene times.

1 | INTRODUCTION

Dating the onset of early Andean mountain building and the coeval formation of the adjacent Andean retroarc foreland basin is of prime interest for understanding the potential role of Andean mountain building in the Cenozoic climate cooling trend. Many studies in Argentina, Bolivia and Colombia suggest that the Andean retroarc foreland basin initiated during late Cretaceous or Palaeocene times (DeCelles, Carrapa, Horton, & Gehrels, 2011; DeCelles & Horton, 2003; Di Giulio et al., 2012; Horton, Hampton, & Waanders, 2001; Nie et al., 2010; Parra, Mora, Lopez, Rojas, & Horton, 2012; Roddaz et al., 2010; Sempéré et al., 1997). However, such studies are lacking for the Peruvian Andes and the adjacent Amazonian retroarc foreland basin. This is partly because obtaining unequivocal evidence of

pre-Neogene Andean shortening is difficult due to the overprinting by younger cratonward advancing deformation and magmatism. One way to constrain the timing of tectonic growth of the Andes is to precisely constrain the first arrival of orogenic-derived detritus in the sedimentary record of the adjacent foreland basin as has been done in the Himalayas (e.g. Hu, Garzanti, Moore, & Raffi, 2015; Zhuang et al., 2015) and in the Colombian Andes (Horton, Parra, et al., 2010, Horton, Saylor, et al., 2010). Hence, dating the shift in provenance from a cratonic to an orogenic source in the Amazonian retroarc foreland basin is of particular interest for determining the timing of the onset of Andean mountain building.

In this study, we provide new biostratigraphic, sedimentological and provenance data to constrain the spatial and chronologic evolution of the southern Peruvian Madre de Dios foreland basin between Maastrichtian and late Palaeocene time. This data set indicates that the Amazonian retroarc foreland basin recorded a late Maastrichtian-late Palaeocene period of Andean mountain building.

2 | BIOSTRATIGRAPHY AND SEDIMENTOLOGY

We characterized the biostratigraphy and depositional environments of a 270-m-thick section of late Cretaceous to late Palaeocene strata exposed in the Madre de Dios Subandean zone (Figure 1a) based on field observations, facies description and the identification of palynomorphs, microfossils and macrofossils at the Naturalis (Leiden, the Netherlands), ISEM (Montpellier, France) and Smithsonian Tropical Research Institute (Panama) laboratories. Detailed sedimentological, palaeontological and palynological descriptions as well as some photographs can be found in the Data Repository.

The lowermost 165 m of the sedimentary section have a late Campanian-early Maastrichtian range (outcrops MD 175 to MD 239 in Figure 1b). MD 175 is late Campanian in age and its palaeontological content further points to a restricted shallow marine environment (Supplementary Data). Above MD 175, reddish shales and palaeosol
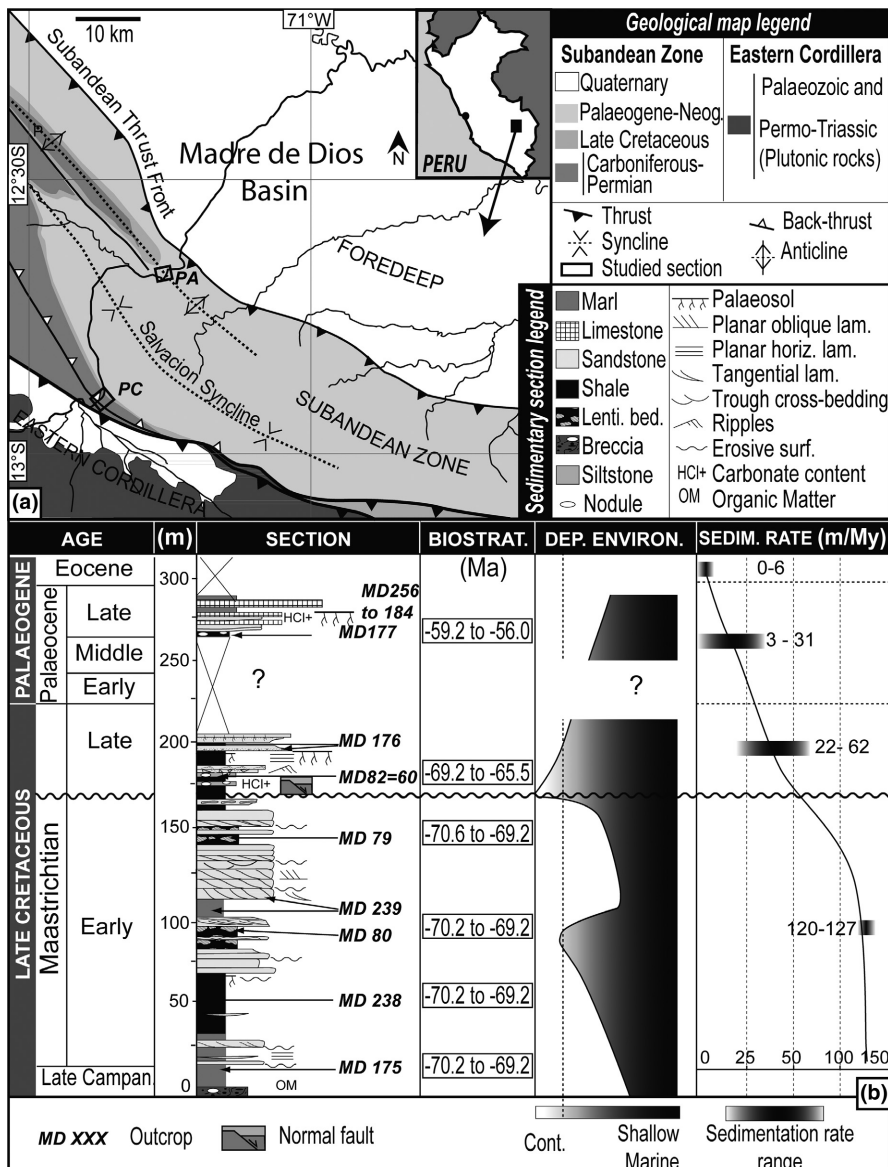
FIGURE 1 (a) Simplified geological map of the studied area. PA: Pantiacolla Anticline; PC: Pongo de Coñeq. See Table S1 in the supplementary data set for sample coordinates. (b) Late Campanian–early Maastrichtian to late Palaeocene Pongo de Coñeq measured stratigraphic section. See text for details

horizons (25–70 m) together with the fossil content of MD 238 indicate an evolution towards a more coastal environment (fluvio-tidal coastal plain). Further up-section, finer-grained blue marls and their palaeontological content (MD 239) reflect a shift to more shallow marine environments. These blue marls pass gradually upwards to vertically stacked 50-cm-thick beds of fine- to medium-grained sandstones (~50 m, 115–165 m) interpreted as tidal compound dunes. Calculated sedimentation rates for the late Campanian early Maastrichtian interval are 120–127 m/Myr (see details in the Data Repository).

Upper Maastrichtian deposits are 40 m thick (165–205 m; Figure 1). The fossil assemblages (samples MD 176 and MD 82=60) indicate a coastal environment with normal salinity (diverse euhaline ichthyofaunas) and continental input (including charophyte oogonia, see Table S2). The lowermost 5 m of the succession consists of reworked material cut by a major erosional surface, overlain by 25 m of thick reddish shales and moderately developed filamentous to nodular carbonate palaeosol horizons. Sediments located above the erosional surface are thus interpreted to be late Maastrichtian strata deposited in a coastal environment that suffered a later subaerial emersion. Further up-section are various 20-cm-thick silty-to-sandy packages alternating with reddish shale. The section evolves upward into breccia levels and channelized coarse- to very-coarse-grained sandstone beds (195–200 m). Upper Maastrichtian strata are deformed by two sets of syn-sedimentary normal faults (average azimuth directions of 171° [family 1] and 354° [family 2] and an average dip of 42°). Late Maastrichtian sedimentation rates were 22–62 m/Myr (see details in the Data Repository).

Above these upper Maastrichtian deposits is a 60-m-thick missing interval of upper Maastrichtian to lower Palaeocene deposits. The lower Palaeocene section (265 290 m) corresponds to estuarine deposits (Facies Association C; Louterbach et al., 2014). Late Palaeocene sedimentation rates range from 3 (non-deposition/erosion) to 31 m/Myr.

Overall, the lower Campanian to lower Palaeocene sedimentary section is a 270-m-thick condensed section corresponding to ~20 Myr and showing sedimentation rates decreasing from ~124 to ~15 m/Myr. These rates are similar to those calculated for similar backbulge to forebulge depozones in Bolivia (Uba, Heubeck, & Hulka, 2006) and Argentina (DeCelles et al., 2011).

3 | PROVENANCE

The major and trace element concentrations and Sr–Nd isotopic composition of selected fine-grained sedimentary rocks (siltstones and mudstones) and zircon U–Pb dating on selected sandstones were used to determine the provenance of the lower Maastrichtian to lower Palaeocene sedimentary succession. Descriptions of samples, processing and analyses as well as detailed results (mineralogy, major and trace element concentrations, Sr–Nd isotopic compositions and U–Pb ages) are provided in the Data Repository.

The mineralogy of the lower Maastrichtian sample is dominated by kaolinite, a mineral that also characterizes the present-day mineralogy of cratonic Amazonian river sediments (Guyot et al., 2007). It has a lower Cr/Th ratio (3.5), higher Th/Sc (1.12) and a more negative Eu anomaly (0.62) than Post-Archaean Australian Shale (McLennan, 2001). Early Maastrichtian deposits are characterized by very negative $\varepsilon Nd(0)$ values lower than −12.7 (−16.4 to −13.9), which are typical for cratonic sedimentary rocks (Nie et al., 2012). They have similar Nd–Sr isotopic composition to the cratonic White Sands Formation (Roddaz, Viers, Brusset, Baby, & Hérail, 2005; Figure 2), further supporting the hypothesis of a cratonic origin. Additional information can be gained from U–Pb ages (Figure 3b). The early Maastrichtian sample has no zircon grains younger than 500 Ma. Main peaks occur at 1.54–1.3 Ga (29.7%), 1.8–1.54 Ga (23.0%) and 1.3–0.9 Ga (21.6%), with minor peaks at 0.7–0.5 Ga (13.5%), 2–1.8 Ga (8.1%) and >2 Ga (4.1%). Zircon populations with age intervals of 2–1.8 Ga and 1.3–0.9 Ga could be derived from the Western Cordillera, as the Ventuari Tapajos and Sunsas cycles are recorded in the Arequipa Massif, southern Peru (see Figure 3a for locations of the diverse provinces) (Bahlburg, Vervoort, DuFrane, Bock, & Augustsson, 2009). However, Rio Negro-Jurunena (1.8–1.55 Ga) and Rondônia-San Ignacio (1.55–1.3 Ga) U–Pb age populations cannot be sourced from the west, as they occur neither in the Arequipa Massif nor in the early Cretaceous Muni Formation (Altiplano-Eastern Cordillera; Perez & Horton, 2014). In addition, a western contribution of the nascent Andes would require the presence of Permo-Triassic and Late Cretaceous U–Pb age populations, such as those observed in the early Cretaceous Muni Formation (Perez & Horton, 2014). Instead, similar contributions from the Rio Negro-Jurunena (1.8–1.55 Ga), Rondônia-San Ignacio (1.55–1.3 Ga) and Sunsas (1.3–0.9 Ga) provinces and a minor contribution from the Ventuari Tapajos Mobile Belt (2–1.8 Ga) require an eastern source from the Amazon craton. There is no obvious source in the Central Peruvian Andes for the 0.7–0.5 Ga zircons
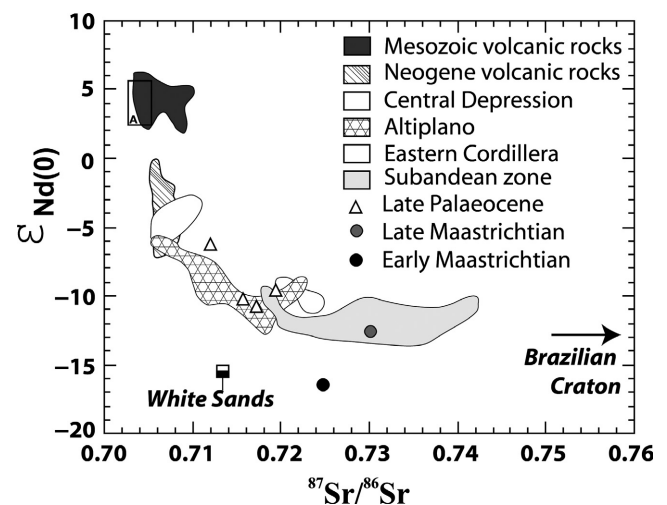
FIGURE 2 $^{87}Sr/^{86}Sr$ versus $\varepsilon Nd(0)$ diagram for Maastrichtian to late Palaeocene samples. References for Mesozoic and Neogene volcanic rocks, Cenozoic sedimentary rocks of the Altiplano and Oriental Cordillera, Subandean zone fields and Peruvian White Sand isotopic compositions can be found in Roddaz et al. (2005)
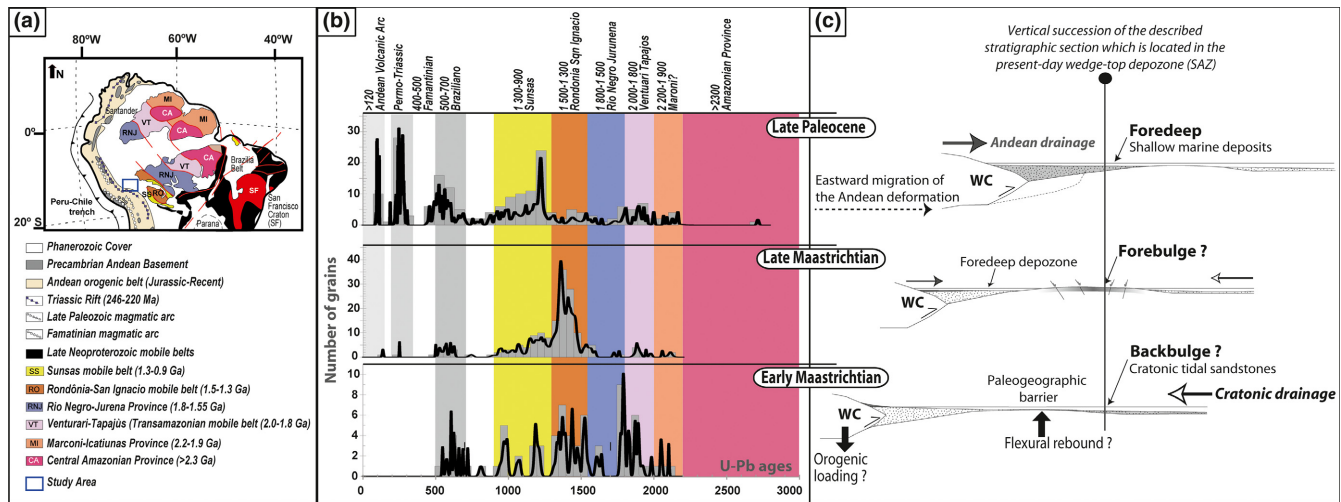
FIGURE 3 (a) Map of South America illustrating the major tectonic provinces and the ages of their most recent metamorphic events, adapted from Chew et al. (2008), Chew et al. (2011), Bahlburg et al., (2009) and Reimann et al. (2010). (b) U–Pb age histograms (grey bars) and probability density functions (black bold curves) of detrital zircons. Cratonic and Andean age domains are taken from Chew et al. (2008), Bahlburg et al. (2009) and Perez and Horton (2014). A total of 74 grains were dated for the Early Maastrichtian (MD 239), 169 grains were dated for the late Maastrichtian (MD 176), and 197 grains were dated for the late Palaeocene (samples MD 85, MD 177, MD 255 and MD 256). U–Pb ages can be found in the supplementary dataset. C: Sketch showing the possible evolution of the southern Amazonian retroarc foreland basin from early Maastrichtian to late Palaeocene times. Sedimentary sources are either Andean or cratonic. Modified from DeCelles and Horton (2003). See text for details [Colour figure can be viewed at wileyonlinelibrary.com]

(Bahlburg et al., 2011; Chew et al., 2008). Hence, following the hypothesis assumed by Chew et al., the 0.7–0.5 Ga zircons could have come either from a Brazilian magmatic arc now buried beneath the present Amazon foreland basin or from the north–south-trending Brasilia Belt located eastward.

The Upper Maastrichtian sample shows an increase in quartz content and a strong decrease in kaolinite content. It has similar Cr/Th and Th/Sc ratios, Eu anomaly and Sr isotopic composition to the early Maastrichtian sample, but less negative εNd(0) values (~−12.6; Figure 2). The upper Maastrichtian sample has a similar Nd–Sr isotopic composition to Neogene sediments in the South Amazonian Foreland Basin (Roddaz et al., 2005), thus indicating a similar provenance. In addition, this εNd(0) value is below the εNd(0) cut-off value of −12.7 that has been used to distinguish between Andean- and Cratonic-derived sedimentary rocks (Nie et al., 2012). The upper Maastrichtian sample shows the first appearance of Cretaceous (0.6%) and Permian (0.6%) zircons. It displays two main peaks at 1.55–1.3 Ga (52.7%) and 1.3–0.9 Ga (27.8%) and a minor peak at 0.7–0.5 Ga (7.1%) (Figure 3b). Zircon grains older than 1.55 Ga account for 11.3% of the population ages. Together with the Nd isotopic composition, the first appearance of Cretaceous and Permian zircons suggests minor Western Andean contributions from the late Permian–Jurassic rift magmatism (Sempéré et al., 2002) and from the Chocolate magmatic arc located in the Peruvian Western Cordillera (Mamani, Worner, & Sempéré, 2010). Dominant contributions from the Rondônia-San Ignacio and Sunsa provinces and diminution of the contribution from an easternmost cratonic source suggest drainage reorganization with contribution from more local sources.

Lower Palaeocene samples are characterized by the appearance of chlorite. They have lower Eu anomalies (0.67–0.76) and lower Th/Sc ratios (0.48–0.80) than those of Maastrichtian sedimentary rocks. They also have less negative εNd(0) values (−10.7 to −6.2) and less radiogenic Sr isotope compositions (between 0.712024 and 0.7190) (Figure 2). The mica–chlorite assemblage characterizes the mineralogy of present-day Andean river sediments (Guyot et al., 2007). Together with low-Eu anomalies and Th/Sc ratios, these results suggest a more abundant input of volcanic detritus in the upper Palaeocene samples compared to the Maastrichtian samples. In Figure 2, the upper Palaeocene samples plot closer to the volcanic arc end-member when compared to the Maastrichtian samples, thus indicating a greater contribution of the Andean magmatic arc. An Andean source is further confirmed by the U–Pb detrital age spectrum (Figure 3b), which shows an increase in the late Permian–Jurassic rift magmatism (15.7% of U–Pb ages) and in Late Cretaceous zircons (5.1%) probably sourced from the Chocolate magmatic arc (Mamani et al., 2010). In this way, Famantinian-aged zircon grains (4.1%) are probably sourced from Palaeozoic shales of the Eastern Cordillera and Altiplano (Reimann et al., 2010). Other peaks are at 1.3–0.9 Ga (32.0%) and 0.7–0.5 Ga (17.3%).

4 | DISCUSSION AND CONCLUSIONS

The shallow marine depositional environment, low-sedimentation rates and large-scale cratonic palaeodrainage during the late Campanian–early Maastrichtian suggest deposition in a low accommodation

setting, in agreement with a backbulge or intracratonic setting (Figure 3c). As early Cretaceous Altiplano and Eastern Cordillera sedimentary rocks already had an Andean contribution (Permo-Triassic and Cretaceous U–Pb age populations; Perez & Horton, 2014), a palaeogeographic barrier preventing the arrival of western Andean-derived detritus probably existed west of the study area by early Maastrichtian times. This topographic barrier might have been formed in response to forebulge flexural uplift due to early Maastrichtian Andean tectonic loading. If correct, coeval upper Campanian–Maastrichtian fluvial conglomerates of the Sicuani-Cuzco basin (Jaillard, 1993) located west of the study area could have constituted the wedge-top deposits of the southern Amazonian retroarc foreland basin system. However, in the absence of detailed basin studies of lower Maastrichtian sedimentary rocks located in the northern Altiplano, it is not possible to fully assess the existence of an early Maastrichtian retroarc foreland basin system in the Central Andes. Upper Maastrichtian deposits are separated from lower Maastrichtian deposits by a subaerial erosive surface, associated with a change in depositional environment from shallow marine to non-marine. This change could be ascribed to the global sea-level fall in the late Maastrichtian (Haq, Hardenbol, & Vail, 1987). However, this cannot explain the presence of syn-sedimentary normal faults and changes in provenance. Syn-sedimentary normal faults associated with the development of palaeosol horizons suggest tectonic-induced emersion that could be related to forebulge uplift (DeCelles et al., 2011; Singh, 2003). A shift towards less negative εNd(0) values indicates a contribution from more juvenile Andean sources such as the magmatic arc and Palaeozoic sedimentary rocks. The first appearance of Cretaceous and Permian zircons further suggests that both the magmatic arc and Permian sedimentary rocks contributed to source the upper Maastrichtian sedimentary rocks. We interpret this result as evidence of an Andean orogenic source. However, the contribution of this source is minor, and the dominant source remains cratonic. Finally, the contribution of the Andean orogenic source increased strongly in the late Palaeocene interval, as attested by the higher percentage of Cretaceous and Permian zircons (47.2%) and by the lower εNd(0) values of analysed sedimentary rocks when compared to Maastrichtian sedimentary rocks. The increasing contribution of Andean orogenic sources associated with tectonic-loading-controlled shallow marine transgression (Louterbach et al., 2014) indicates that Andean mountain building was ongoing in late Palaeocene times. To conclude, our data suggest a minimum late Maastrichtian age for the onset of the Amazonian retroarc foreland basin system. Our data also suggest that no topographic barrier, and hence forebulge, existed at the present-day locus of the Eastern Cordillera (between the Altiplano and the SAZ), contrary to the findings of Carlotto (2013). Together with previous studies in Colombia (Nie et al., 2010; Parra et al., 2012), Bolivia (Sempéré et al., 1997) and Argentina (Di Giulio et al., 2012), our data suggest that the erosion of the Andean mountain belt may have started in the late Cretaceous and especially that the Andean retroarc foreland basin system was active by late Maastrichtian–late Palaeocene times in response to Andean Cordillera loading.

ORCID

Mélanie Louterbach iD http://orcid.org/0000-0001-8987-2208

REFERENCES

Bahlburg, H., Vervoort, J. D., DuFrane, S. A., Bock, B., & Augustsson, C. (2009). Timing of accretion and crustal recycling at accretionary orogens: Insights learned from the western margin of South America. *Earth-Science Reviews*, *97*, 227–253.

Bahlburg, H., Vervoort, J. D., DuFrane, S. A., Carlotto, V., Reimann, C., & Cárdenas, J. (2011). The U-Pb and Hf isotope evidence of detrital zircons of the Ordovician Ollantaytambo Formation, southern Peru, and the Ordovician provenance and paleogeography of southern Peru and northern Bolivia. *Journal of South American Earth Sciences*, *32*, 196–209. https://doi.org/10.1016/j.jsames.2011.07.002

Carlotto, V. (2013). Paleogeographic and tectonic controls on the evolution of Cenozoic basins in the Altiplano and Western Cordillera of southern Peru. *Tectonophysics*, *589*, 195–219. https://doi.org/10.1016/j.tecto.2013.01.002

Chew, D. M., Magna, T., Kirkland, C. L., Miskovíc, A., Cardona, A., Spikings, R. A., & Schaltegger, U. (2008). Detrital zircon fingerprint of the Proto-Andes: Evidence for a Neoproterozoic active margin? *Precambrian Research*, *167*, 186–200. https://doi.org/10.1016/j.precamres.2008.08.002

DeCelles, P. G., Carrapa, B., Horton, B. K., & Gehrels, G. E. (2011). Cenozoic foreland basin system in the central Andes of northwestern Argentina: Implications for Andean geodynamics and modes of deformation. *Tectonics*, *30*: TC6013.

DeCelles, P. G., & Horton, B. K. (2003). Early to middle Tertiary foreland basin development and the history of Andean crustal shortening in Bolivia. *Geological Society of America Bulletin*, *115*, 58–77. https://doi.org/10.1130/0016-7606(2003)115<0058:ETMTFB>2.0.CO;2

Di Giulio, A., Ronchi, A., Sanfilippo, A., Tiepolo, M., Pimentel, M., & Ramos, V. (2012). Detrital zircon provenance from the Neuquén Basin (south-central Andes): Cretaceous geodynamic evolution and sedimentary response in a retroarc foreland basin. *Geology*, *40*, 559–562.

Guyot, J. L., Jouanneau, J. M., Soares, L., Boaventura, G. R., Maillet, N., & Lagane, C. (2007). Clay mineral composition of river sediments in the Amazon Basin. *Catena*, *71*, 340–356. https://doi.org/10.1016/j.catena.2007.02.002

Haq, B. U., Hardenbol, J., & Vail, P. R. (1987). Chronology of fluctuating sea levels since the Triassic. *Science*, *235*, 1156–1167. https://doi.org/10.1126/science.235.4793.1156

Horton, B. K., Hampton, B. A., & Waanders, G. L. (2001). Paleogene syn-orogenic sedimentation in the Altiplano plateau and implications for initial mountain building in the central Andes. *Geological Society of America Bulletin*, 113, 1387–1400. https://doi.org/10.1130/0016-7606(2001)113<1387:PSSITA>2.0.CO;2

Horton, B. K., Parra, M., Saylor, J. E., Nie, J., Mora, A., Torres, V., ... Strecker, M. R. (2010). Resolving uplift of the northern Andes using detrital zircon age signatures. *GSA Today*, 20, 4–9. https://doi.org/10.1130/GSATG76A.1

Horton, B. K., Saylor, J. E., Nie, J., Mora, A., Parra, M., Reyes-Harker, A., & Stockli, D. F. (2010). Linking sedimentation in the northern Andes to basement configuration, Mesozoic extension, and Cenozoic short-ening: evidence from detrital zircon U-Pb ages, Eastern Cordillera, Colombia. *Geological Society of America Bulletin*, 122, 1423–1442. https://doi.org/10.1130/B30118.1

Hu, X., Garzanti, E., Moore, T., & Raffi, I. (2015). Direct Stratigraphic dating of India-Asia collision onset at the Selandian (Middle Paleocene, 59 ± 1 Ma). *Geology*, 43, 859–862. doi:10.1130/G36872.1. https://doi.org/10.1130/G36872.1

Jaillard, E. (1993). L'évolution tectonique de la marge péruvienne au Sénonien et Paléocène et ses relations avec la géodynamique. *Bulletin de la Société Géologique de France*, 164, 819–830.

Louterbach, M., Roddaz, M., Bailleul, J., Antoine, P. O., Adnet, S., Kim, J. H., ... Baby, P. (2014). Evidences for a late Paleocene marine incursion in Southern Amazonia (Madre de Dios Sub-Andean Zone, Peru). *Palaeogeography, Palaeoclimatology, Palaeoecology*, 414, 451–471. https://doi.org/10.1016/j.palaeo.2014.09.027

Mamani, M., Worner, G., & Sempéré, T. (2010). Geochemical variations in igneous rocks of the Central Andean orocline (13 degrees S to 18 degrees S): tracing crustal thickening and magma generation through time and space. *Geological Society of America Bulletin*, 122, 162–182. https://doi.org/10.1130/B26538.1

McLennan, S. M. (2001). Relationships between the trace element composition of sedimentary rocks and upper continental crust. *Geochemistry Geophysics Geosystems*, 2, –2000GC000109.

Nie, J., Horton, B. K., Mora, A., Saylor, J. E., Housh, T. B., Rubiano, J., & Naranjo, J. (2010). Tracking exhumation of Andean ranges bounding the Middle Magdalena Valley Basin, Colombia. *Geology*, 38, 451–454. https://doi.org/10.1130/G30775.1

Nie, J., Horton, B. K., Saylor, J. E., Mora, A., Mange, M., Garzione, C. N., ... Parra, M. (2012). Integrated provenance analysis of a convergent retroarc foreland system: U-Pb ages, heavy minerals, Nd isotopes, and sandstone compositions of the Middle Magdalena Valley basin, northern Andes, Colombia. *Earth-Science Reviews*, 110, 111–126. https://doi.org/10.1016/j.earscirev.2011.11.002

Parra, M., Mora, A., Lopez, C., Rojas, L. E., & Horton, B. K. (2012). Detecting earliest shortening and deformation advance in thrust-belt hinterlands: Example from the Colombian Andes. *Geology*, 40, 175–178. https://doi.org/10.1130/G32519.1

Perez, N. D., & Horton, B. K. (2014). Oligocene-Miocene deformational and depositional history of the Andean hinterland basin in the northern Altiplano plateau, southern Peru. *Tectonics*, 33, 1819–1847. https://doi.org/10.1002/2014TC003647

Reimann, C. R., Bahlburg, H., Kooijman, E., Berndt, J., Gerdes, A., Carlotto, V., & López, S. (2010). Geodynamic evolution of the early Paleozoic western Gondwana margin 14°–17°S reflected by the detritus of the Devonian and Ordovician basins of Southern Peru and Northern Bolivia. *Gondwana Research*, 18, 370–384. https://doi.org/10.1016/j.gr.2010.02.002

Roddaz, M., Hermoza, W., Mora, A., Baby, P., Parra, M., Christophoul, F., ... Espurt, N. (2010). Cenozoic sedimentary evolution of the Amazonian foreland basin system. In C. Hoorn, & F. P. Wesselingh (Eds.), *Amazonia, landscape and species evolution: A look into the past*, (pp. 61–88). Hoboken: Wiley-Blackwell, Oxford, Bleckwell-Wilew.

Roddaz, M., Viers, J., Brusset, S., Baby, P., & Hérail, G. (2005). Sediment provenances and drainage evolution of the Neogene Amazonian foreland basin. *Earth and Planetary Science Letters*, 239, 57–78. https://doi.org/10.1016/j.epsl.2005.08.007

Sempéré, T., Butler, R. F., Richards, D. R., Marshall, L. G., Sharp, W., & Swisher, C. C. (1997). Stratigraphy and chronology of upper Cretaceous lower Paleogene strata in Bolivia and northwest Argentina. *Geological Society of America Bulletin*, 109, 709–727. https://doi.org/10.1130/0016-7606(1997)109<0709:SACOUC>2.3.CO;2

Sempéré, T., Carlier, G., Soler, P., Fornari, M., Carlotto, V., Jacay, J., ... Jiménez, N. (2002). Late Permian–Middle Jurassic lithospheric thinning in Peru and Bolivia, and its bearing on Andean-age tectonics. *Tectonophysics*, 345, 153–181. https://doi.org/10.1016/S0040-1951(01)00211-6

Singh, B. P. (2003). Evidence of growth fault and forebulge in the Late Paleocene (57.9–54.7 Ma), western Himalayan foreland basin, India. *Earth and Planetary Science Letters*, 216, 717–724. https://doi.org/10.1016/S0012-821X(03)00540-5

Uba, C. E., Heubeck, C., & Hulka, C. (2006). Evolution of the late Cenozoic Chaco foreland basin, Southern Bolivia. *Basin Research*, 18, 145–170. https://doi.org/10.1111/bre.2006.18.issue-2

Zhuang, G., Najman, Y., Guillot, S., Roddaz, M., Antoine, P.-O., Métais, G., ... Solangi, S. H. (2015). Constraints on the Collision and the pre-collision tectonic configuration between India and Asia from detrital geochronology, thermochronology, and geochemistry studies in the lower Indus basin, Pakistan. *Earth and Planetary Science Letters*, 432, 363–373. https://doi.org/10.1016/j.epsl.2015.10.026

SUPPORTING INFORMATION

Additional Supporting Information may be found online in the supporting information tab for this article.

Figure S1 Rare earth element (REE) concentrations normalized against Post Archaean Australian Shales.

Figure S2 (left) and Figure S3 (right): Evolution of sedimentation rates through time, for each of the 8 cases (left) and for the minimum and maximum computed sedimentation rates.

Figure S4 Detailed sedimentological section drawn from field observations, from upper Campanian to Palaeocene strata.

Table S1 Outcrop references for this study.

Table S2 Palaeontological content of the sedimentary rocks analyzed in this work.

Table S3 Mineralogical composition and relative abundance of analyzed mudstones.

Table S4 Nd–Sr systematics of analyzed sedimentary rocks.

Table S5 Major and trace element concentrations of analyzed sedimentary rocks.

Table S6 U–Pb zircon geochronology analysis: Laser-Ablation Multicollector ICP Mass Spectrometry for MD 239.

Table S7 U–Pb zircon geochronology analysis: Laser-Ablation Multicollector ICP Mass Spectrometry for MD 176.

Table S8 U–Pb zircon geochronology analysis: Laser-Ablation Multicollector ICP Mass Spectrometry for MD 177.

Table S9 U–Pb zircon geochronology analysis: Laser-Ablation Multicollector ICP Mass Spectrometry for MD 255.

Table S10 U–Pb zircon geochronology analysis: Laser-Ablation Multicollector ICP Mass Spectrometry for MD 256.

Table S11 U–Pb zircon geochronology analysis: Laser-Ablation Multicollector ICP Mass Spectrometry for MD 85.

Table S12 Numbers and percentages of U–Pb age dates representing known and distinct geochronological events in probable source regions on the Amazonia craton and in the central Andes.

Table S13 The different sedimentation rates calculated by Petro-Mod 1D software for each case.

Table S14 Details of each studied case used to compute the sedimentation rates through time.

Photo S1 Campanian to lower Maastrichtian blue marl deposits.

Photo S2 Close up of sample MD 175 (late Campanian).

Photo S3 Lower Maastrichtian tidal sandstones.

Photo S4 Tidal compound dune.

Photo S5 Outcrop photo of the erosive surface separating the lower and upper Maastrichtian deposits and the palaeosol that developed immediately above.

Photo S6 Close up of the palaeosol in Photo S5.

Photo S7 Syn-sedimentary normal faults affecting the upper Maastrichtian deposits.

Photo S8 MD 176 sandstone sampled for U–Pb dating.